Evaluation of Advanced Microwave Sounding Unit Tropical-Cyclone Intensity and Size Estimation Algorithms

JULIE L. DEMUTH

Department of Atmospheric Science, Colorado State University, and Cooperative Institute for Research in the Atmosphere, Fort Collins, Colorado

MARK DEMARIA

NOAA/NESDIS, Fort Collins, Colorado

JOHN A. KNAFF

Cooperative Institute for Research in the Atmosphere, Fort Collins, Colorado

THOMAS H. VONDER HAAR

Department of Atmospheric Science, Colorado State University, and Cooperative Institute for Research in the Atmosphere, Fort Collins, Colorado

(Manuscript received 9 October 2002, in final form 18 August 2003)

ABSTRACT

Advanced Microwave Sounding Unit (AMSU) data are used to provide objective estimates of 1-min maximum sustained surface winds, minimum sea level pressure, and the radii of 34-, 50-, and 64-kt (1 kt $\equiv$ 0.5144 m s^{-1}) winds in the northeast, southeast, southwest, and northwest quadrants of tropical cyclones. The algorithms are derived from AMSU temperature, pressure, and wind retrievals from all tropical cyclones in the Atlantic and east Pacific basins during 1999–2001. National Hurricane Center best-track intensity and operational radii estimates are used as dependent variables in a multiple-regression approach. The intensity algorithms are evaluated for the developmental sample using a jackknife procedure and independent cases from the 2002 hurricane season. Jackknife results for the maximum winds and minimum sea level pressure estimates are mean absolute errors (MAE) of 11.0 kt and 6.7 hPa, respectively, and rmse of 14.1 kt and 9.3 hPa, respectively. For cases with corresponding reconnaissance data, the MAE are 10.7 kt and 6.1 hPa, and the rmse are 14.9 kt and 9.2 hPa. The independent cases for 2002 have errors that are only slightly larger than those from the developmental sample. Results from the jackknife evaluation of the 34-, 50-, and 64-kt radii show mean errors of 30, 24, and 14 n mi, respectively. The results for the independent sample from 2002 are generally comparable to the developmental sample, except for the 64-kt wind radii, which have larger errors. The radii errors for the 2002 sample with aircraft reconnaissance data available are all comparable to the errors from the jackknife sample, including the 64-kt radii.

1. Introduction

Upon discontinuation of aircraft reconnaissance in the western North Pacific Ocean in 1987, the Atlantic Ocean became the only tropical-cyclone basin with routine in situ tropical-cyclone (TC) observations. The worldwide standard for TC intensity monitoring, especially when reconnaissance data are not available, is based on a method developed by Dvorak (1975) and enhanced in the mid-1980s (Dvorak 1984). The Dvorak technique uses visible and IR satellite imagery to observe the central and banding features of TCs and cloud-top temperatures near the eye. Although the methods are augmented by a set of empirical rules, interpretations of TC attributes are subjective and can result in different intensity estimates of the same storm. The technique generally is successful, but large errors sometimes are possible. Velden et al. (1998) extended Dvorak's work, developing an automated version of the IR method—the objective Dvorak technique (ODT)—for which the only subjectivity is the user's selection of the storm-center location. Although their rmse is only 8.34 hPa, the ODT is not applicable to tropical depressions (TD) or weak tropical storms (TS), and further limitations exist when a central dense overcast is present. These

Corresponding author address: Mark DeMaria, NOAA/NESDIS/ORA, CIRA/Colorado State University, West Laporte Ave., Fort Collins, CO 80523.
E-mail: mark.demaria@noaa.gov

works suggest that it is advantageous to have an alternative TC intensity estimation technique that is independent of the Dvorak method.

Operational forecast centers, such as the National Hurricane Center (NHC), are also required to estimate the radial extent of 34-, 50-, and 64-kt (1 kt $\equiv$ 0.5144 m s^{-1}) surface winds at 6-h intervals. Wind radii observations are obtained from reconnaissance data, ship reports, buoys, or satelliteborne scatterometers, but many of these data sources have spatial limitations or occur opportunistically. In their absence, conservative overestimates of the wind radii commonly are reported as symmetric circular and semicircular values when large asymmetries may actually exist. The applicability of scatterometers for wind observations has led to a surge in their usage, yet Jones et al. (1999) note many effects that degrade the wind retrieval accuracy, especially near the region of peak winds.

Because of the shortcomings of estimating TC intensity and wind structure, an alternate method is desired that is entirely objective and is applicable to TDs, TSs, and hurricanes. Passive microwave remote sensing is suitable for TC studies because 1) microwaves penetrate most clouds beyond the top layer, a beneficial feature when a central dense overcast exists; 2) microwaves are unaffected by hydrometeor contamination, except in heavily precipitating regions; and 3) microwave sensing is not limited to a certain time of day.

Several studies have capitalized on the utility of microwave sensing for tropical cyclone analysis after the pioneering work by Kidder (1979) and Kidder et al. (1978, 1980). Bankert and Tag (2002) describe an objective TC intensity estimation method that uses Special Sensor Microwave Imager (SSM/I) 85-GHz imagery and derived rain rates. Although their technique shows promise, the rmse is on the order of 20 kt for independent data. Merrill (1995) used Microwave Sounding Unit (MSU) and Special Sensor Microwave Temperature Sounder (SSM/T) data to estimate TC minimum sea level pressure (MSLP). The primary limitation of his technique was the poor horizontal resolution, which, at best, is 110 km for MSU data and 175 km for SSM/T data.

In May of 1998, the MSU's successor, the Advanced Microwave Sounding Unit (AMSU), was launched aboard the *National Oceanic and Atmospheric Administration* (*NOAA*)*-15* satellite. The multiplatform AMSU has more channels (15 on AMSU-A and 5 on AMSU-B) and increased horizontal resolution (48 and 16 km at nadir for AMSU-A and -B, respectively) relative to the MSU. AMSU-A primarily is for providing temperature soundings, but it also is useful in deriving other TC parameters, including cloud liquid water and rain rate. AMSU-B primarily is for providing moisture soundings. For more details of the AMSU instrument and tropical-cyclone applications, see Kidder and Vonder Haar (1995) and Kidder et al. (2000).

Despite its advantages, one limitation of using AMSU data for TC analysis is the temporal resolution. The AMSU instrument passes over the same location a maximum of 2 times daily. However, the deployment of three additional AMSU instruments—aboard *NOAA-16* (launched in September of 2000), *Aqua* (May of 2002), and *NOAA-17* (June of 2002)—helps to alleviate this problem.

The efficacy of the AMSU for TC analysis has prompted several recent studies. Spencer and Braswell (2001) statistically related six AMSU-derived parameters to the maximum winds of Atlantic TCs. Their results, reported as the average error standard deviation, correspond closely with reconnaissance data (9.1 kt) but degrade markedly (14.6 kt) for cases without aircraft observations. Similar to Merrill (1995), Brueske and Velden (2003) developed a TC estimation algorithm that uses 55-GHz AMSU data to estimate MSLP. Their method includes a correction for subsampled upper-tropospheric warm anomalies (UTWA) that uses AMSU-B data to estimate eye size. However, their retrievals are sensitive to the eye-size parameter, and a version of their algorithm is under development in which the eye size is determined by other methods.

In this study, a method is described for estimating TC intensity—measured by 1-min maximum sustained winds (MSW) and MSLP—and size (with the wind radii), utilizing AMSU-A data from 1999 to 2001. AMSU-A temperature retrievals are used to determine the geopotential height and surface pressure fields from the hydrostatic equation, and the gradient wind equation is used to estimate the tangential wind. Parameters from these fields are used as input to statistical relationships for estimation of the MSW, MSLP, and azimuthally averaged (AA) radii of 34-, 50-, and 64-kt winds. The asymmetric wind radii are determined by fitting the mean wind radii to the sum of an idealized symmetric vortex and an asymmetry factor related to the storm motion. A jackknifing procedure is used for evaluation of the intensity estimates against NHC postseason best-track (BT) data, and wind radii estimates are evaluated against NHC operational TC forecast advisories. Evaluations are performed for the entire developmental sample and a subset of the 100 cases with coincident aircraft reconnaissance observations. An independent evaluation is performed for cases from the 2002 tropical season.

2. Data

The AMSU-A (hereinafter referred to as AMSU) radiances were collected in real time for all storms in the Atlantic and east Pacific basins during the 1999–2001 tropical-cyclone seasons. *NOAA-15* data were available from 1999 to 2001, and additional data from *NOAA-16* were collected in 2001. Current and 12-h-old TC position estimates at 6-hourly intervals from the NHC are interpolated to the time of the most recent AMSU data, which typically is within 6 h of the current storm po-

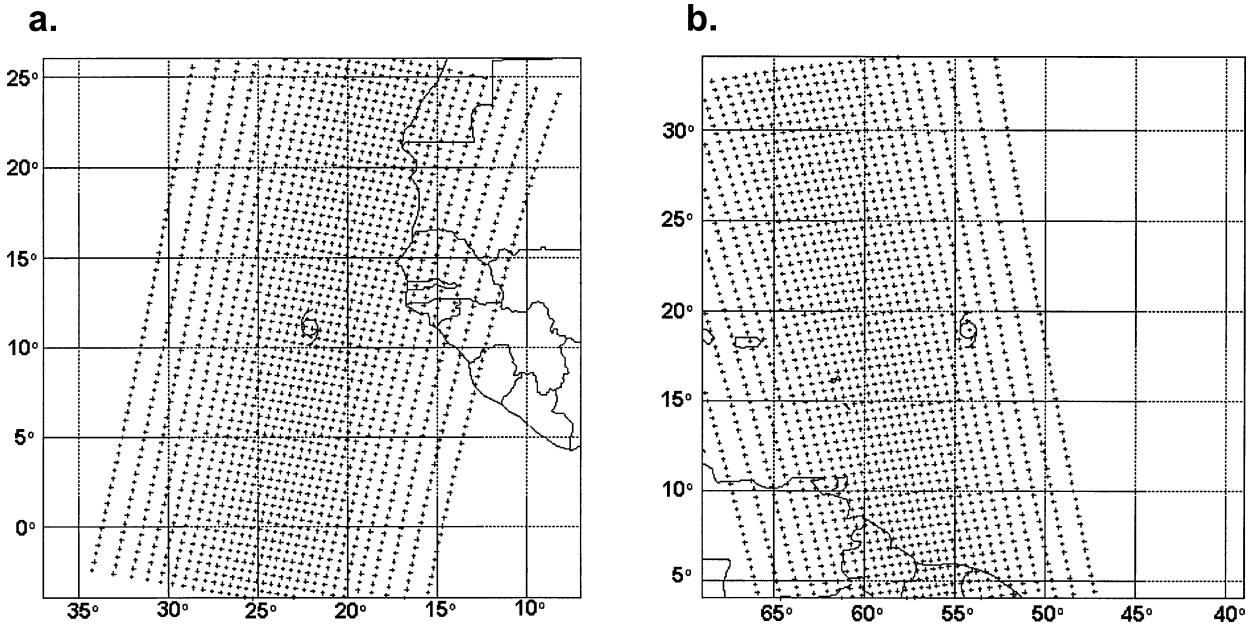

FIG. 1. A portion of the AMSU swath showing (a) Hurricane Isaac near nadir on 21 Sep 2000 and (b) Hurricane Gert near the 600-km threshold of the swath center on 16 Sep 1999.

sition estimate. Although the cross-track-scanning AMSU swaths are nearly 2200 km wide, the sample was limited to those cases in which the storm center fell within 600 km of the swath center. The AMSU data are analyzed over a domain with a 600-km radius (chosen to include the gale radius of the largest Atlantic tropical cyclones) so that when the storm center falls at or near the 600-km threshold there is a small portion of the analysis domain with no data; this situation is not problematic because the analysis procedure extrapolates data from neighboring data points. The maximum resolution (48 km) occurs when the storm is near the center of the AMSU data swath. At 600 km from the swath center, the data resolution is approximately 80 km. Figure 1 shows examples of the data coverage for storms near and 600 km from the center of the AMSU swath.

a. The temperature retrieval

Prior to the temperature retrieval, two corrections to the *NOAA-15* data were made for scan position and viewing angles (Goldberg et al. 2001). For *NOAA-16,* only the viewing angle correction was applied because the scan position correction was negligible for that satellite (M. D. Goldberg 2002, personal communication). After the corrections, the normalized radiances were used as input to a statistical temperature retrieval (Goldberg et al. 2001; Knaff et al. 2000), which provides temperature as a function of pressure at 40 levels from 1000 to 0.1 hPa. Only the 23 pressure levels between 920 and 50 hPa were used, because the 1000-hPa level generally is below the surface in the center of strong TCs, and 50 hPa was assumed to be above the storm circulation. The cloud liquid water (CLW) also is estimated from the AMSU-A data as part of the statistical retrieval algorithm.

Although microwave soundings provide information below the cloud-top layer, utilization in strongly convective regions of TCs is problematic because of hydrometeor attenuation. Because of their relatively large sizes, CLW droplets and ice crystals absorb and scatter microwave radiation, resulting in anomalously cold retrieved temperatures and errors in the derived pressure field. Preliminary investigations of the retrieved fields showed these detrimental effects (Figs. A2a,c,e); thus, two corrections—one for attenuation by CLW and one for ice scattering—were developed as described in the appendix.

The initial CLW correction was applied to the temperature profiles at the AMSU swath points. A two-pass distance-weighted analysis method (Barnes 1964) then was applied to interpolate the unevenly spaced temperature and CLW data on the swath to an evenly spaced $12^\circ \times 12^\circ$ grid with 0.2° grid spacing. This process smoothes the data, the degree to which is controlled by the *e*-folding radius in the Barnes analysis. The magnitude of the *e*-folding radius was chosen based upon the behavior of the response function and by experimentation. Values of 50–150 km were tested, and it was found that the minimum value that sufficiently smoothed the retrieved fields (determined subjectively from contour plots) was 100 km, and so this value was used for all of the Barnes analyses. Note, however, that the statistical intensity estimation procedure described in section 3 was not very sensitive to the choice of the *e*-folding radius within the range of 75–150 km. After

interpolation of temperature and CLW to the grid, the second hydrometeor correction was applied for ice scattering (appendix).

b. The wind retrieval

The horizontal wind retrieval assumes hydrostatic and gradient balance. The hydrometeor-corrected temperatures at the 23 pressure levels were interpolated to a radial grid and azimuthally averaged, with the TC center located at the origin, so that temperature is a function of pressure and radius, extending outward 600 km. Surface temperature cannot be derived from the AMSU, and so it was obtained from the National Centers for Environmental Prediction (NCEP) global analysis closest in time to the AMSU swath, though not more than 6 h old. The AMSU algorithm is insensitive to the NCEP surface temperatures, because they are used only as a lower boundary condition to derive the surface pressure. Nearly the entire surface pressure gradient comes from the temperature structure above the surface through the downward integration of the hydrostatic equation.

Next, the geopotential height field was derived as a function of pressure using the hydrostatic equation. In doing so, additional assumptions were made that 1) temperature varies linearly with height between two pressure levels, 2) variations in gravity with height can be neglected so that height and geopotential height are equivalent, and 3) virtual temperature effects can be neglected. The last assumption could cause errors of a few hectopascals in the surface pressure, which might have been reduced by using AMSU-B moisture profiles. However, the AMSU-B instrument on *NOAA-15* was not functioning properly, and so the data were not available consistently before 2001. Nevertheless, errors in the pressure gradient from neglecting virtual temperature effects are proportional to the moisture gradient rather than to the total moisture. The moisture gradient errors are less than those of the total moisture.

The hydrostatic integration was begun at the surface at the outer radius of the domain, where the surface pressure boundary condition was determined from the same NCEP analysis used for the surface temperature. This equation was integrated upward to 50 hPa to give the heights at the AMSU pressure levels at radius $r =$ 600 km. A final assumption then was made that the 50-hPa level is above all perturbations associated with the TC so that the height of this level is constant at all radii. The hydrostatic equation then was integrated downward from 50 to 920 hPa at all radii in the interior of the domain. With the height and temperature of the 920-hPa level and the surface temperature from NCEP, the hydrostatic equation then was integrated downward to compute the surface pressure at all points in the domain. Again, assuming a linear variation in temperature with height between the AMSU pressure levels, the temperature and pressure as a function of height were calculated at 1-km intervals from the surface to 20 km, and the density at each level was calculated with the ideal gas equation.

With the pressure p and density ρ known as a function of height and r, the wind field was determined assuming gradient balance [(1)], where the radial pressure gradient was calculated using centered finite differences (with one-sided differences at $r = 0$ and 600 km), the Coriolis parameter f was evaluated at the storm center, and V is the wind speed:

$$\frac{V^2}{r} + fV = \frac{1}{\rho}\frac{\partial p}{\partial r} \quad \text{and} \tag{1}$$

$$V = \frac{-rf}{2} \pm \sqrt{\left(\frac{rf}{2}\right)^2 + \frac{r}{\rho}\frac{\partial p}{\partial r}}. \tag{2}$$

Sometimes, the radial pressure gradient in (2) is large and negative, preventing a real solution of the gradient wind equation; for these points, the magnitude of the pressure gradient was reduced until the radicand was positive, providing a real solution.

An example of the AMSU-retrieved temperature perturbation and gradient winds for Hurricane Gert is shown in Fig. 2. The anomalies were calculated at each level by subtracting the retrieved temperatures at $r =$ 600 km from the temperature at each radius. The hurricane had MSW of 115 kt at this time; however, the coarse resolution of the AMSU and the smoothing of the data resulted in retrieved MSW of approximately 60 kt. The retrieved UTWA of approximately 6°C also is likely a tempered estimate of the true magnitude.

c. AMSU cases

The temperature, pressure, and gradient winds as a function of radius and height and the CLW as a function of latitude and longitude were determined from AMSU data for all available cases from 1999 to 2001. Cases in which the storm center was within 100 km of a major landmass were excluded so that at least one AMSU footprint in all directions from the storm center was over water.

Figure 3 summarizes the developmental sample, in which the reported intensities are from the NHC best track. The distribution of storm intensities in the developmental dataset was representative of climatological conditions. The sample included 473 cases from 89 TCs, of which 247 were from the Atlantic and 226 were from the east Pacific. Over two-thirds are at TD (123 cases) and TS (199 cases) intensities, and the remaining cases are hurricane strength (151 cases). Of the latter, 102 are category-1 or -2 storms (65–95 kt) and 49 are category-3 or -4 storms (100–135 kt); there were no cases of category-5 TCs (>135 kt) during an AMSU overpass. The number of cases for estimating the wind radii is reduced, as will be discussed in section 4, leaving 129 cases from 31 TCs for the 34-kt wind radii, 92 cases

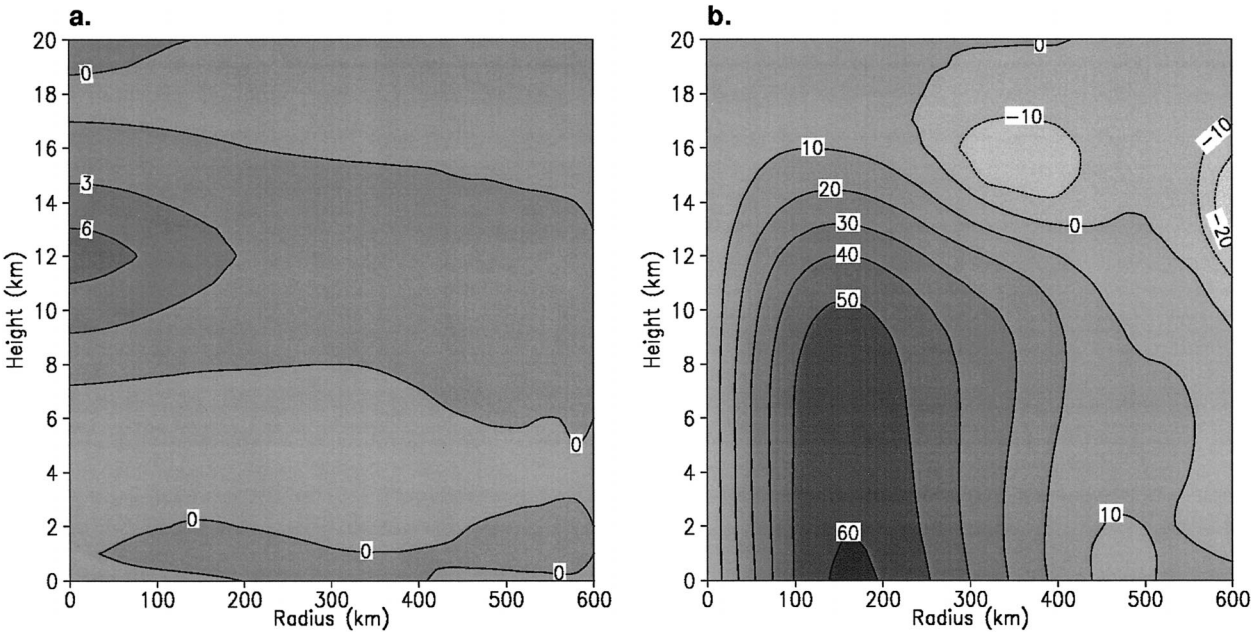

FIG. 2. Radial–height cross sections for Hurricane Gert on 16 Sep 1999 of AMSU-retrieved (a) temperature anomalies (°C), showing the warm core at a height of approximately 12 km, and (b) gradient winds (kt), showing that the MSW occur at approximately 175 km from the storm center. The data locations for this case are shown in Fig. 1b.

from 23 TCs for the 50-kt wind radii, and 68 cases from 19 TCs for the 64-kt wind radii.

The independent sample from 2002 includes 288 cases (143 Atlantic and 145 east Pacific) from 30 TCs, of which 64 cases were within 6 h of reconnaissance. Ninety-five cases are TDs, 140 are TSs, and 53 are hurricanes. Of the latter, 36 are category 1 or 2 and 17 are category 3 or higher. For the wind radii estimations, there were 218 cases from 24 TCs for the 34-kt wind radii, 120 cases from 16 TCs for the 50-kt wind radii, and 67 cases from 10 TCs for the 64-kt wind radii.

3. Tropical-cyclone intensity estimation

Although the horizontal resolution of the AMSU is more than 2 times as good as that of the MSU, it still is too coarse to observe tropical cyclones without subsampling problems. The eye diameters of Atlantic tropical cyclones range from 8 to over 200 km, but the majority fall between 30 and 60 km (Weatherford and Gray 1988). Even if a TC falls near the nadir position, the 48-km resolution is not sufficient to resolve the tight pressure gradient near the radius of maximum wind. However, several parameters can be derived from the AMSU temperature, pressure, and wind retrievals. As shown in this study, when combined with other parameters available in real time, these data can be related statistically to NHC-reported MSW and MSLP, providing objective estimates of each. The development of these algorithms is explained in this section, followed by an evaluation with the dependent sample and an independent sample from 2002.

a. Methods

Eighteen parameters derived from the AMSU data and one additional non-AMSU-derived parameter available in real time served as possible estimators of tropical-cyclone intensity (Table 1). The parameters relay information from various vertical levels about retrieved pressures, winds, temperature anomalies, swath spacing, and cloud liquid water values. The combined 19 parameters make up the independent variables used as potential estimators of TC intensity through the MSW and MSLP; except for the area-averaged CLW percentage (CLWPER), all AMSU-derived parameters were azimuthally averaged.

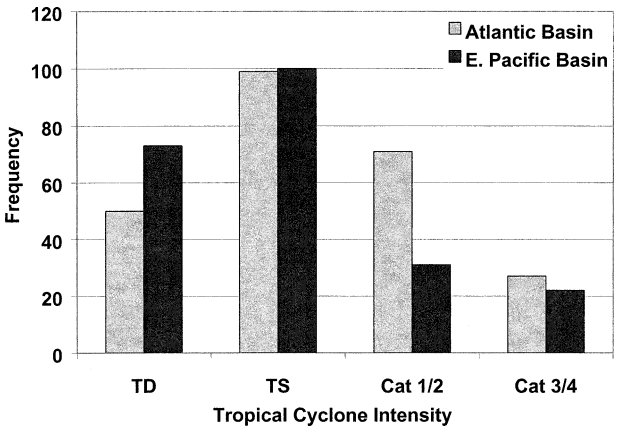

FIG. 3. Histogram of all AMSU cases from 1999 to 2001, binned by intensity and basin of occurrence.

TABLE 1. Potential estimators of tropical cyclone intensity, where r is the radius and z is height.

Potential intensity estimators	Description
MINP	Min surface pressure (hPa) at storm center
DP0	Pressure drop (hPa) at the surface from $r = 600$ to 0 km
DP3	Pressure drop (hPa) at $z = 3$ km from $r = 600$ to 0 km
TMAX	Max temperature perturbation (°C), calculated as the temperature at $r = 600$ km minus the temperature at each radius
ZMAX	Height (km) of max temperature perturbation (TMAX)
SS	Resolution (km) of AMSU footprint at storm center (swath spacing)
VMX0	Max wind speed (kt) at the surface
RMX0	Radius (km) of max winds at the surface
VMX3	Max wind speed (kt) at $z = 3$ km
RMX3	Radius (km) of max winds at $z = 3$ km
VBI0	Tangential winds at surface, averaged from $r = 0$ to 250 km
VBI3	Tangential winds at $z = 3$ km, averaged from $r = 0$ to 250 km
VBI5	Tangential winds at $z = 5$ km, averaged from $r = 0$ to 250 km
VBO0	Tangential winds at surface, averaged from $r = 250$ to 500 km
VBO3	Tangential winds at $z = 3$ km, averaged from $r = 250$ to 500 km
VBO5	Tangential winds at $z = 5$ km, averaged from $r = 250$ to 500 km
CLWAVE	CLW content (mm), averaged from $r = 0$ to 100 km
CLWPER	Percentage of area with CLW values >0.5 mm from $r = 0$ to 300 km
LAT*	Lat from NHC at storm center, interpolated to AMSU swath time

* LAT is the only parameter not derived from AMSU data.

The dependent data for the TC intensity estimations are from the NHC BT linearly interpolated to the time of the AMSU swath. However, the best-track data are not all ''ground truth''; the intensity estimates are determined from available Dvorak satellite estimates, ship reports, buoy data, land stations, aircraft reconnaissance measurements (nearly all of which are from the Atlantic), satellite cloud-track winds, and scatterometer and passive microwave (SSM/I) surface winds. Although a developmental dataset consisting entirely of in situ data is preferable, AMSU and reconnaissance data were coincident within 6 h only 100 times from 1999 to 2001. There is a marginal amount of cases from which to develop a statistical algorithm with 19 potential estimators, and so, until a larger dataset becomes available, the best-track data are the best alternative for stable development. The reconnaissance dataset was used for a separate evaluation.

All of the parameters in Table 1 are probably relevant to TC intensity, but the actual significance of each one is not explicit. Therefore, the relationship between the estimators and the predictands was analyzed with multiple linear regressions. In general, it is not prudent to include every possible estimator in the regression equation, because some may not be valuable in estimating the predictand or some may be mutually correlated, providing redundant information. The list of potential estimators was consequently shortened initially by correlating each variable against the predictands. If the correlation coefficient was less than 0.5, then that variable was excluded initially.

A backward stepwise regression with a 1% significance level ($\alpha = 0.01$) then was used to select a set of estimators from the remaining variables. It is possible, though, that some variables removed by the initial correlation step could improve the variance explained: although a given variable may not be correlated with the MSW or the MSLP, it may be correlated with the residuals of the estimative algorithms. For instance, the AMSU footprint resolution at the storm center (SS) has no direct physical relationship to TC intensity, but as the resolution worsens, the intensity is underestimated by the AMSU data. Thus, there is a relationship between SS and the residuals from the backward stepwise regression. To avoid excluding these relevant connections, each of the variables removed by the initial correlation was analyzed against the residuals, and if a relationship existed, the variable was added back to the potential estimator pool. Then the backward stepwise regression was reanalyzed, and the variables retained were the final set used in the algorithms to estimate the MSW and the MSLP.

The intensity estimators selected using the 1999–2001 data were evaluated using a ''storm jackknife'' procedure. The typical jackknife method develops regression equations on $n - 1$ cases and tests the algorithm on the withheld case. However, usually there are numerous cases from one TC, potentially weighting the developmental dataset and underestimating the error on the ''independent'' case. To prevent this bias, all cases for a given storm were withheld, the algorithms to estimate the MSW and MSLP were developed with the remaining cases, and then the algorithms were tested independently on all the withheld cases from that storm.

b. Results

1) DEPENDENT DATA RESULTS

The final regression equation for MSW contains seven AMSU-derived estimators, explaining 72.3% of the var-

TABLE 2. Regression variables and their corresponding coefficients, normalized coefficients, and p values retained to estimate best-track reports of MSW (kt) and MSLP (hPa).

Independent variable	Max sustained winds (kt) $R^2 = 72.3\%$			Min sea level pressure (hPa) $R^2 = 76.5\%$		
	Coef	Normalized coef	p value	Coef	Normalized coef	p value
MINP	—	—	—	0.623	0.259	0.000
DP0	−1.648	−0.459	0.000	1.521	0.602	0.000
TMAX	2.996	0.204	0.008	−2.777	−0.269	0.000
SS	0.191	0.070	0.005	−0.145	−0.076	0.001
RMX3	−0.020	−0.069	0.006	0.014	0.072	0.002
VBI5	4.109	0.883	0.000	−2.492	−0.760	0.000
CLWAVE	19.556	0.327	0.000	−12.499	−0.297	0.000
CLWPER	−0.222	−0.168	0.000	0.116	0.124	0.001

iance ($R/^2$); an additional parameter is retained to explain 76.5% of the variance in the MSLP (Table 2).

To compare the coefficients for each estimator, normalized coefficients were calculated from nondimensional dependent and independent variables calculated by mean centering and then dividing by the standard deviation. Each normalized coefficient has a comparable magnitude for MSW and MSLP, suggesting that the parameters work similarly in estimating each; the signs are opposite, however, because MSW and MSLP are inversely related. The normalized coefficients illustrate that the AMSU-derived tangential wind at a height of 5 km from 0 to 250 km (VBI5) is the most influential parameter in estimating both MSW and MSLP, followed closely by the pressure drop at the surface (DP0). VBI5 probably was selected instead of the comparable variables at 3 km (VBI3) or at the surface (VBI0) because the height and wind fields in the domain interior are derived by a downward integration, and noise and errors accumulate near the surface. In addition, hydrometeor effects worsen closer to the surface. As expected, DP0 is an influential parameter because the pressure drop is strongly related to intensity.

The two estimators with lower normalized coefficients, SS and the radius of maximum winds at 3 km (RMX3), were the only ones added back to the estimator pool by the residual analyses. Although SS is not physically related to TC intensity, it helps to correct for resolution variations by increasing the estimated intensity when SS is large. In a similar way, the estimated intensity decreases as RMX3 increases because the AMSU better resolves larger storms. RMX3 probably was chosen over the comparable variable at the surface (RMX0) for the same reasons described above for VBI5.

The mean absolute error MAE (rmse) on the development dataset is 10.6 (13.5) kt for estimating MSW and 6.5 (8.8) hPa for MSLP (Table 3). These statistics deteriorate only slightly on the storm jackknife data, suggesting that the artificial skill is minimal. The rmse of 14.1 kt for the MSW estimates is smaller than Bankert and Tag's (2002) rmse of 19.7 kt. The rmse of the MSLP is 9.3 hPa, which is 1.0 hPa higher than the reported ODT rmse (Velden et al. 1998). However, if one restricts the AMSU cases to only Atlantic storms as Velden et al. did, the resultant rmse of 8.2 hPa is comparable to their findings. The standard deviation of the MSW jackknife residuals is 14.1 kt, akin to 14.6 kt from Spencer and Braswell (2001). Therefore, the intensity estimation equations developed in this study have errors comparable to those from other methods, with the advantage that they estimate MSW and MSLP for tropical disturbances of all strengths. However, a homogeneous sample would be necessary for a true comparison of all methods.

When the storm jackknife estimates were evaluated only for the 100 cases with reconnaissance data within 6 h, all but one of the statistical measures improves (Table 3). The MSW explained variance increased to 74.3%, and the MAE and standard deviation of the residuals decreased to 10.7 and 13.7 kt, respectively. However, the rmse increased slightly to 14.9 kt for the aircraft cases, likely signifying that there are a few cases with large errors, which are skewing the rmse on this smaller dataset, but that there are many more cases with

TABLE 3. Comparison of the results for estimations of MSW (kt) and MSLP (hPa) using the AMSU-derived intensity algorithms for the developmental, storm jackknife, and storm jackknife against reconnaissance datasets.

	Developmental dataset ($n = 473$)		Jackknife dataset ($n = 473$)		Jackknife data against reconnaissance data ($n = 100$)	
	MSW	MSLP	MSW	MSLP	MSW	MSLP
R^2	72.3%	76.5%	70.2%	73.9%	74.3%	83.1%
MAE	10.6	6.5	11.0	6.7	10.7	6.1
Rmse	13.5	8.8	14.1	9.3	14.9	9.2
Std dev of residuals	13.5	8.8	14.1	9.3	13.7	9.0

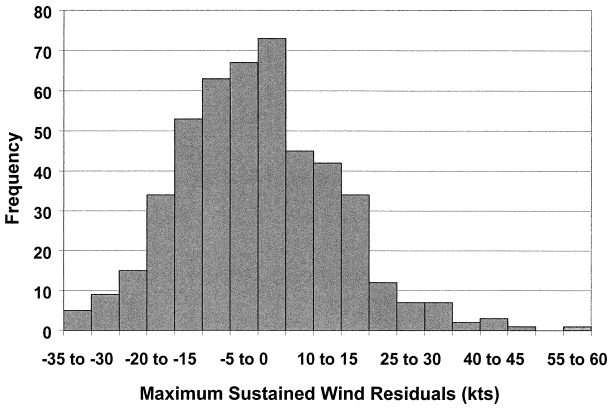

FIG. 4. Histogram of residuals (best track minus AMSU estimated) for estimates of MSW (kt) from 1999–2001 storm jackknife data.

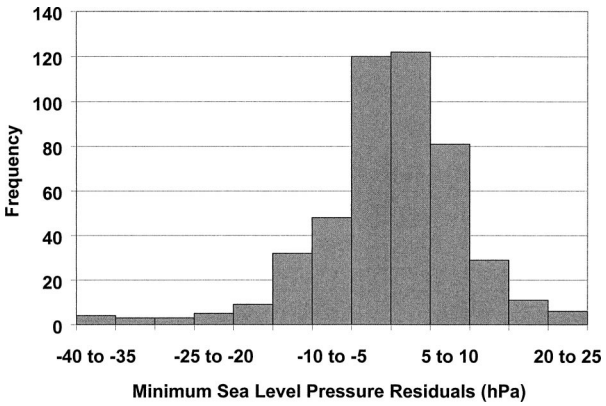

FIG. 5. Same as Fig. 4, but for MSLP (hPa).

small errors, keeping the MAE down and raising the coefficient of determination. For the cases with reconnaissance data, the MSLP explained variance increased to 83.1%, the MAE (rmse) decreased slightly to 6.1 (9.2) hPa, and the residual standard deviation decreased to 9.0 hPa.

The distribution of residuals (Fig. 4) shows that 72.5% of the errors fall within 15 kt and only 13% of errors are more than 20 kt. For the MSLP estimates, the residual distribution (Fig. 5) shows that 78.4% lie within 10 hPa, with only 4.4% exceeding 20 hPa. The fact that the maximum wind error exceeded 20 kt in only about 13% of the cases is encouraging. Brown and Franklin (2002) showed that the errors in the Dvorak estimates exceed 20 kt in about 10% of the cases. These results suggest that the AMSU can provide intensity estimates that are comparable to the Dvorak method but are independent of visible and IR imagery. Because of this independence, a method that included both types of data would likely lead to even more accurate intensity estimates.

A closer examination of the residuals revealed six storms that were underestimated by the AMSU algorithm by in excess of 30 kt, with a maximum error of 57 kt. One-half of these storms were from Hurricane Iris, and another was from Hurricane Juliette. Based upon their appearance in IR imagery, both were small storms. In fact, aircraft data for Iris near the time of its peak intensity indicated a radius of maximum wind as small as 8 km. These results indicate that the algorithm does not perform well in such cases because of its limited horizontal resolution. The other two underestimated cases were from Hurricane Lenny, which may have been ill-affected by inaccurate temperature retrievals in and around the elevated terrain of the Caribbean islands. In addition, it appeared that the AMSU footprint locations occurred on either side of the warm core associated with the storm, so that the most intense region was not sampled.

There are 14 cases in which the AMSU algorithm overestimates TC intensity by more than 25 kt, the greatest overestimation being 32.4 kt. These large overestimations likely occur for two reasons: 1) when TCs intensify rapidly, the warm core appears to increase faster than the surface winds, and 2) when TCs lose all convection, the warm core is exposed. The latter occurs most often in the east Pacific, which is where 64% of the large overestimations occurred. A possible way to correct this error would be to use IR data as part of a multisensor algorithm.

2) INDEPENDENT DATA RESULTS

To evaluate further the intensity AMSU estimation, the algorithm developed from the 1999–2001 cases was run in real time during the 2002 hurricane season, and results were compared with the 2002 NHC postseason best track. As shown in Table 4, the performance of the algorithm is robust, with only a slight increase in error relative to the developmental dataset. The algorithms explain 69.0% of the MSW variance and 67.5% of the MSLP variance. Furthermore, the MAE (rmse) is 10.9 (14.1) kt for estimating the MSW and 7.5 (10.5) hPa for estimating the MSLP. When evaluated against only the 64 cases from 2002 with reconnaissance data, the results again are consistent with the developmental dataset, with 72.3% and 83.4% of the variance explained for MSW and MSLP, respectively. In addition, the MAE

TABLE 4. Comparison of the results for independent estimations of MSW (kt) and MSLP (hPa) using the AMSU-derived intensity algorithms for all 2002 data and only data with reconnaissance.

	Best-track cases (n = 288)		Reconnaissance cases (n = 64)	
	MSW	MSLP	MSW	MSLP
R^2	69.0%	67.5%	72.3%	83.4%
Bias	2.2	−1.1	−4.7	5.3
MAE	10.9	7.5	11.0	7.0
Rmse	14.1	10.5	14.3	10.6
Std dev of residuals	13.9	10.4	13.6	9.2

TABLE 5. Regression variables and their corresponding coefficients, normalized coefficients, and *p* values retained to estimate NHC reports of the azimuthally averaged 34-, 50-, and 64-kt wind radii (n mi).

Independent variable	Coef	Normalized coef	*p* value
Azimuthally averaged 34-kt wind radii (n mi) R^2 = 71.9%			
MINP	−3.788	−0.718	0.000
VBI5	−3.135	−0.349	0.005
LAT	2.100	0.327	0.000
BTMSW*	1.113	0.501	0.000
Azimuthally averaged 50-kt wind radii (n mi) R^2 = 65.9%			
TMAX	9.461	0.526	0.006
VMX0	1.273	0.525	0.004
VMX3	−2.059	−0.772	0.001
VBO5	2.298	0.300	0.004
CLWPER	0.620	0.321	0.002
Azimuthally averaged 65-kt wind radii (n mi) R^2 = 80.8%			
TMAX	6.286	0.623	0.000
SS	0.427	0.168	0.005
CLWPER	0.270	0.248	0.010
BTMSW*	0.217	0.188	0.005

* BTMSW is the best-track estimate of the maximum sustained winds; in real time, the operational estimate will be used.

and rmse of the reconnaissance-only evaluation are very similar to the errors of the entire 2002 dataset.

4. Tropical-cyclone wind radii estimation

Similar to the intensity estimation, a statistical procedure that utilizes AMSU-derived parameters was employed to estimate the AA radii of 34-, 50-, and 64-kt winds. The AMSU-derived AA estimates subsequently were used with a simple surface wind model—given as the sum of a constant vector proportional to TC motion plus a modified Rankine vortex—to make asymmetric estimations of the wind radii in the northeast (NE), southeast (SE), southwest (SW), and northwest (NW) quadrants relative to the TC center, as are reported by the NHC operational forecast advisories every 6 h. The developments of the symmetric and asymmetric wind radii techniques are described in this section; the former are cross evaluated with the same storm jackknife procedure used for the intensity evaluation, and the asymmetric estimates were evaluated against the NHC advisories closest in time to the AMSU swath data (with a maximum 3-h difference) for both the developmental and the 2002 independent datasets.

TABLE 7. Comparison of the results for estimating the asymmetric wind radii (n mi) of 34-, 50-, and 64-kt winds using AMSU-derived estimates of the azimuthally averaged wind radii with a Rankine vortex model; all quadrants have been combined into one sample.

	34-kt asymmetric radii (n = 129)	50-kt asymmetric radii (n = 92)	64-kt asymmetric radii (n = 68)
R^2	58.6%	44.0%	55.1%
MAE	30.2	23.9	14.1
(% of avg)	(27.0%)	(36.1%)	(37.5%)
Rmse	40.8	34.2	18.7
Bias	−3.2	−5.2	0.1

a. Methods

The NHC operational MSW estimates, as opposed to the AMSU-estimated MSW, were used to determine which wind radii were to be estimated. For example, if the operational estimate of the MSW is 65 kt, the 34-, 50-, and 64-kt wind radii all are to be estimated, even if the AMSU estimate is below 65 kt. This method was used to maintain consistency with the NHC's reported TC intensity estimate.

The same 19 parameters used for the intensity estimation (Table 1) and the operational estimate of intensity itself make up the independent variables (estimators) for the AA 34-, 50-, and 64-kt wind radii estimations. The dependent variable, reported in nautical miles (n mi), is the average of the four wind radii from the operational forecast advisories issued every 6 h by the NHC. The radii closest in time to the AMSU swath were used with no more than a 3-h difference. Because there is no systematic technique analogous to the Dvorak method for estimating the wind radii from satellite data, the wind radii data in the NHC advisories are derived from surface and remotely sensed data and from aircraft reconnaissance data. As with the best-track data, the majority of the ground-truth data for the wind radii are not in situ measurements. Unlike the BT intensities, however, there is no postseason analysis of the wind radii, suggesting that large errors may be inherent in the developmental dataset. Therefore, the data for devel-

TABLE 6. Comparison of the results for estimating the azimuthally averaged 34-, 50-, and 64-kt wind radii (n mi) with AMSU-derived algorithms (Dev) for the developmental and storm jackknife datasets (Jack).

	34-kt azimuthally averaged radii (n = 129)		50-kt azimuthally averaged radii (n = 92)		64-kt azimuthally averaged radii (n = 68)	
	Dev	Jack	Dev	Jack	Dev	Jack
R^2	71.9%	65.4%	65.9%	39.3%	80.8%	73.7%
MAE	21.2	24.3	17.9	25.7	8.0	9.4
(% of avg)	(19.0%)	(21.7%)	(26.9%)	(38.7%)	(21.2%)	(25.0%)
Rmse	28.3	31.6	23.3	32.6	10.1	11.8
Bias	—	1.0	—	−9.9	—	−0.1

TABLE 8. Comparison of the results, shown by quadrant, for estimating the asymmetric wind radii (n mi) of 34-, 50-, and 64-kt winds using AMSU-derived estimates of the azimuthally averaged wind radii with a Rankine vortex model.

	NE	SE	SW	NW
		34-kt asymmetric wind radii		
R^2	59.5%	66.9%	60.9%	45.7%
MAE	28.4	28.9	30.5	32.8
Rmse	38.4	39.0	41.8	43.9
Bias	−13.1	−1.8	11.5	−9.3
		50-kt asymmetric wind radii		
R^2	33.9%	67.3%	52.8%	26.6%
MAE	29.2	21.8	19.3	25.4
Rmse	41.2	29.6	27.0	37.1
Bias	−15.8	−2.8	4.4	−6.8
		64-kt asymmetric wind radii		
R^2	69.0%	59.5%	44.3%	55.5%
MAE	15.3	12.0	14.7	14.4
Rmse	18.9	17.0	19.1	19.6
Bias	−5.0	6.3	3.9	−4.6

oping the wind radii equations were restricted to Atlantic cases west of 55°W, which have the best coverage of aircraft reconnaissance, buoys, ships, and island stations. The east Pacific cases that had reconnaissance data also were included.

The same four-step statistical method with the same significance levels used in developing the intensity estimation algorithms was used to create three wind radii algorithms, one each for the AA 34-, 50-, and 64-kt winds. After the initial correlation (removing those with a coefficient less than 0.5) of each estimator with the predictand, a backward stepwise regression was employed with the resulting variables ($\alpha = 0.01$), followed by an examination of the residuals against the parameters removed at the outset by the correlation. Again, any parameters showing a relationship with the residuals were added back to the potential estimator pool, and the regression was reanalyzed.

With the AMSU-derived AA wind radii estimates, the wind radii in the NE, SE, SW, and NW quadrants were determined by using a modified Rankine vortex (Depperman 1947) applied to a polar coordinate system, where the surface wind speed V outside the radius of MSW r_m is given by a simple model,

$$V(r, \theta) = (V_m - \gamma)\left(\frac{r}{r_m}\right)^{-x} + \gamma \cos(\theta - \theta_0), \quad (3)$$

where r is the radius from the TC center, θ is the angle measured from a direction 90° to the right of the storm heading, V_m is the maximum wind, γ is the asymmetry factor resulting from the storm translational speed (Schwerdt et al. 1979), and x is a unitless, positive number that determines the rate at which the wind speed decays with radius. Application of (3) to the best-track MSW and observed wind radii in each quadrant for the 1999–2000 sample indicated that the best fit is obtained when γ is 60% of the asymmetry factor from Schwerdt's equation, and $\theta_0 = 0$, indicating that the MSW generally are 90° to the right of the direction of motion.

With θ_0 and γ specified and V_m set to the operational estimate of MSW, the AMSU-estimated AA wind radii then were used to determine the two remaining free parameters, r_m and x, by solving (3) for r and applying an azimuthal average to give

$$\bar{r} = \frac{r_m}{2\pi} \int_0^{2\pi} \left[\frac{V_m - \gamma}{V - \gamma \cos(\theta - \theta_0)}\right]^{1/x} d\theta. \quad (4)$$

There are three possible scenarios for finding r_m and x: 1) when the MSW of a TC is greater than 34 but less than 50 kt, providing only an AMSU estimate of the AA 34-kt wind radii; 2) when the MSW is greater than 50 but less than 64 kt, resulting in AMSU estimates of the AA 50- and 64-kt wind radii; and 3) when the MSW is greater than 64 kt, providing all three AMSU estimates of the AA wind radii. The second case is ideal in that (4) can be evaluated twice, once each for the AA 34- and 50-kt wind radii, resulting in two equations for the two unknowns r_m and x. The dilemmas occur when the MSW is less than 50 kt, because only the mean 34-kt wind radius is known, and when the wind is 64 kt or greater, because three average wind radii are available.

To remedy these problems, the parameters x and r_m were determined using a variational approach in which a cost function, $C(r_m, x)$, is minimized. The cost function is given by

$$C = \frac{(r_{34} - R_{34})^2}{\sigma_{34}^2} + \frac{(r_{50} - R_{50})^2}{\sigma_{50}^2} + \frac{(r_{64} - R_{64})^2}{\sigma_{64}^2} + \lambda_x \frac{(x - x_c)^2}{\sigma_x^2} + \lambda_{\mathrm{rm}} \frac{(r_m - r_{mc})^2}{\sigma_{\mathrm{rm}}^2}, \quad (5)$$

where r_{34} is the average 34-kt wind radius determined from (4), R_{34} is the 34-kt wind radius from the statistical algorithm, σ_{34} is the standard deviation of a sample of mean 34-kt wind radii (and similar for the 50- and 64-kt wind radii), x_c is the climatological value of x, r_{mc} is the climatological value of r_m, and σ_x and σ_{rm} are the sample standard deviations of x and r_m, respectively. The climatological variables and standard deviations were determined from NHC operational estimates of wind radii for all Atlantic storms from 1988 to 2000 west of 55°W. The standard deviations in (5) are constants, but the climatological values of x and r_m are a function of the TC MSW, where r_{mc} decreases and x_c increases for stronger storms.

The last two terms on the right side of (5) are ''penalty terms'' that prevent the values of x and r_m from deviating too far from the climatological values as determined by λ_x and λ_{rm}. Values of 0.1 for both parameters were cho-

sen based upon an analysis of the behavior of the minimization of (5) for idealized wind profiles. The penalty terms have only a small influence on the solution except in the special cases in which the storm maximum wind is very close to one of the wind radii thresholds (34, 50, or 64 kt) and the speed of motion is large. In these cases, the wind radii are zero for a fairly large span of azimuth for the highest wind threshold, making the azimuthal mean radius in (4) very small. In the minimization procedure, unrealistic values of x and r_m are required to compensate. The penalty terms prevent this unrealistic solution from being selected.

Once r_m and x are known, (3) is used to determine the radius for any wind speed V at any azimuth θ. The value of V is set, depending on which wind radii magnitude is sought (e.g., when determining the asymmetric 34-kt wind radii, $V = 34$), and θ is determined by rotating the desired geographic direction into the storm-motion relative coordinate system.

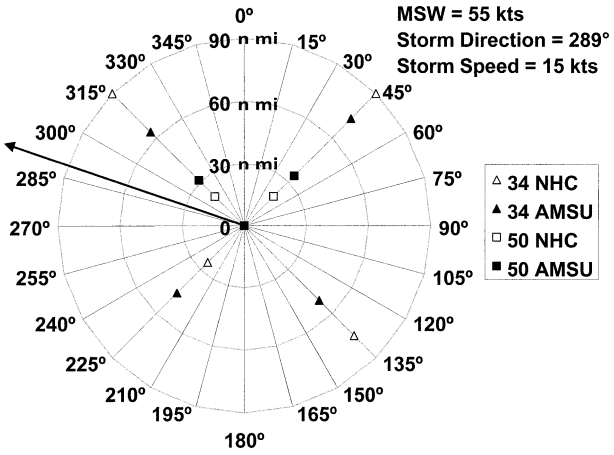

FIG. 6. Comparison of AMSU-derived and NHC reports of asymmetric 34- and 50-kt wind radii (n mi) for Tropical Storm Iris (1152 UTC 6 Oct 2001), where the arrow denotes direction of storm translation.

b. Results

1) AZIMUTHALLY AVERAGED WIND RADII

The final regressions include from four to five variables (Table 5) that account for approximately 66%–81% of the variations in the 34-, 50-, and 64-kt AA wind radii. The set of estimative parameters varies based on which wind radius is being approximated. The 50- and 64-kt radii equations have two estimators in common; the 50- and 34-kt radii equations have no common estimators.

Table 6 shows the error statistics for the wind radii estimates for the developmental and storm jackknife samples. For the AA 34- and 64-kt wind radii, the results of the jackknife dataset decline modestly, suggesting that the AMSU-derived algorithms are without artificial skill. However, the 50-kt wind radii are not estimated as well. There is large scatter ($R^2 = 39.3\%$) and a bias of -9.9 n mi, indicating an underestimate of the 50-kt wind radii. It is possible that part of this error is due to uncertainties in the NHC estimates of the wind radii; this ambiguity will be resolved once a large enough reconnaissance dataset is acquired for comparison. However, the lower reliability of the AA 50-kt wind radii is less of a problem when the asymmetric wind radii are calculated, because the cost function combines this information with the AA 34- and 64-kt wind radii.

2) ASYMMETRIC WIND RADII

(i) Dependent data results

The AMSU-derived asymmetric wind radii estimates generally compare well to the NHC asymmetric wind radii (Tables 7 and 8), although large differences sometimes occurred (the maximum differences are on the order of 200 n mi for the 34-kt radii, 150 n mi for 50-kt radii, and 90 n mi for 64-kt wind radii). The assumption that the wind field asymmetries are solely the result of motion may be the cause of such large differences, particularly when a storm is imbedded in an environment that contains strong horizontal wind shear. Once again, without a dataset consisting only of in situ observations, it is difficult to determine whether outliers are due to the statistical estimation or to uncertainties in the NHC evaluation data.

To illustrate better the asymmetric wind radii estimation, two specific examples are discussed below: 1) a small but highly asymmetric storm that validates well with concurrent reconnaissance data and 2) a large storm without concurrent aircraft reconnaissance data.

On 1152 UTC 6 October 2001, Tropical Storm Iris had MSW of 55 kt and was moving west-northwest at 15 kt. Because Iris was south of the Greater Antilles, reconnaissance data were coincident with this time. With an intensity so close to the 50-kt wind radii threshold and a rapid translation speed, 50-kt winds are not expected to encircle the TC; rather, they exist only in the NE and NW quadrants (Fig. 6). Both the AMSU-derived and NHC radii estimates show this asymmetry very well, although they differ in magnitude by about 10 n mi.

The case of Hurricane Gert on 1132 UTC 22 September 1999 shows how uncertainties in the evaluation data complicate the assessment of errors. The NHC radii estimates for this case were almost exactly the same as those determined from a reconnaissance flight nearly 36 h prior. However, between the flight and the time of this case, the TC weakened from 95 to 70 kt and the speed of motion increased from 9 to 21 kt. There consequently were no 64-kt winds in the NW or SW quadrants from the AMSU data, and yet the NHC continued to report 64-kt wind radii of 90 and 50 n mi, respectively, in those quadrants (Fig. 7). Without in situ observations,

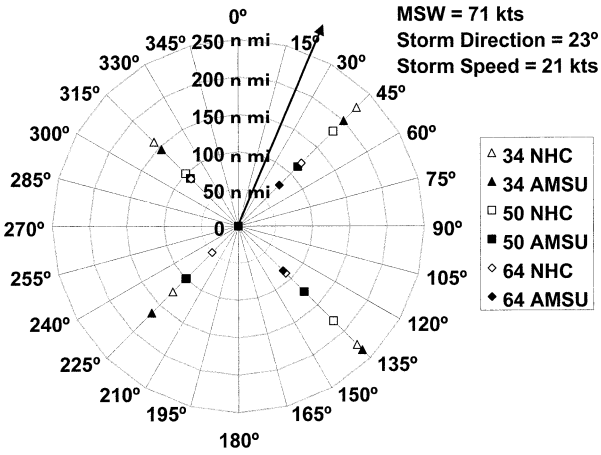

FIG. 7. Similar to Fig. 6, but for asymmetric 34-, 50-, and 64-kt wind radii (n mi) for Hurricane Gert (1132 UTC 22 Sep 1999).

it is unclear which radii estimates are more accurate in this case.

Despite the uncertainties in the NHC wind radii for Hurricane Gert, both the AMSU and NHC 34- and 50-kt radii are much larger for Gert than for Iris (Figs. 6 and 7). Based upon aircraft data and satellite imagery, Gert was a much larger storm than Iris, indicating that the AMSU algorithm can distinguish between storms of different sizes. In addition, the radius of maximum wind is estimated as part of the asymmetric wind radii estimation procedure; although these parameters were not evaluated in this study, the values for these Gert and Iris examples were 69 and 29 n mi, respectively, again distinguishing between the large and small storms.

(ii) Independent data results

Table 9 shows the radii error statistics for the 2002 independent sample. Comparing Tables 7 and 9 shows that the errors of the AMSU estimates of the 34- and 50-kt asymmetric wind radii for the 2002 independent cases are comparable to the results with the jackknife sample, although the biases are a little larger. For the 64-kt radii, the performance for the total 2002 sample degrades in comparison with the jackknife results, but the performance for the 2002 sample with reconnaissance data is comparable. It is possible that the degradation of the 64-kt radii estimates for the total 2002 sample is partially due to uncertainties in the operational radii estimates, because this sample includes east Pacific as well as Atlantic storms. The 64-kt wind radii are the most difficult to estimate without aircraft data because the satellite winds [Quick Scatterometer (QuikSCAT) and SSM/I] are less valid for higher wind speeds, and generally there are fewer in situ data near the storm center. When a large enough sample becomes available, the radii algorithm should be rederived and evaluated using only those cases that include aircraft reconnaissance as ground truth. Nevertheless, the general consistency of the radii errors between the jackknife and independent samples suggests that the performance of the algorithm was not overly influenced by the choice of the developmental sample, and the method provides radii estimates that explain 45%–60% of the variability of the NHC operational estimates.

TABLE 9. Comparison of the results for independent estimations of the asymmetric wind radii (n mi) of 34-, 50-, and 64-kt winds for 2002 data using AMSU-derived estimates of the azimuthally averaged wind radii with a Rankine vortex model; all quadrants have been averaged into one. Results are shown for all cases and for cases in which reconnaissance observations were made within 3 h of the AMSU observation.

	All cases		
	34-kt asymmetric radii (n = 218)	50-kt asymmetric radii (n = 120)	64-kt asymmetric radii (n = 67)
R^2	48.5%	58.5%	15.5%
MAE	35.3	12.3	38.0
Rmse	45.9	19.2	48.9
Bias	−16.9	0.2	−15.5
	Reconnaissance cases		
	34-kt asymmetric radii (n = 39)	50-kt asymmetric radii (n = 24)	64-kt asymmetric radii (n = 8)
R^2	50.7%	53.1%	60.3%
MAE	37.7	16.8	12.3
Rmse	48.1	28.4	16.9
Bias	−15.8	1.7	10.4

5. Summary and conclusions

This study used AMSU data to estimate two measures of TC intensity—MSW and MSLP—and wind structure through the azimuthally averaged radii of 34-, 50-, and 64-kt winds. The physically based part of the algorithm provides a spatially smoothed view of the tropical cyclone, which is input to statistical models to provide the intensity and radii estimates. The estimative algorithms were developed with cases from 1999 to 2001 with a correlation–multiple-linear-regression-residual analysis technique, and a storm jackknife evaluation was employed to assess the error characteristics. The azimuthally averaged wind radii subsequently were used in conjunction with a simple surface wind model (the sum of a modified Rankine vortex and a constant vector proportional to the storm motion) to estimate the wind radii in the NE, SE, SW, and NW quadrants. The intensity estimates were evaluated with postseason best-track analyses; for the wind radii, evaluation was made with NHC operational forecast advisory estimates. In addition to the jackknife evaluations with the developmental sample, an evaluation was performed using an independent sample from the 2002 hurricane season.

In general, the intensity estimates in this study have errors comparable to those of the objective Dvorak method—with the advantage of providing intensity estimates for all ranges of storm intensity—and to those from other AMSU-based intensity techniques. An ad-

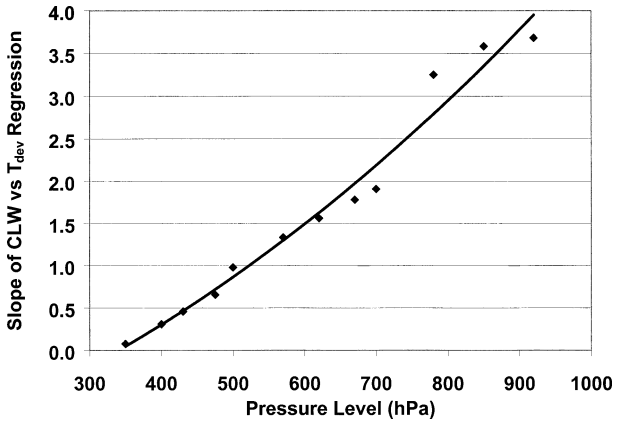

FIG. A1. The slope of the CLW-vs-temperature-deviation regression vs the corresponding pressure level, fit with a quadratic curve.

vantage of the current technique, however, is that it also provides estimates of the radii of 34-, 50-, and 64-kt winds. These radii estimates explain 45%–60% of the variability of the wind radii in the operational NHC forecast advisories.

Work is under way to extend the intensity and wind radii estimation algorithms globally to all other tropical basins. Other future work may include enhancing the asymmetric wind estimations by using a nonlinear balance equation to derive the three-dimensional wind field, rather than forcing the maximum wind to be 90° to the right of the storm motion, thus accounting for cases in which the tropical cyclone is embedded in an environment that contains strong horizontal wind shear. AMSU-B and IR imagery also may be used to determine TC size so that the AMSU-derived estimative parameters can be scaled accordingly. Last, when a sufficient number of AMSU cases with coincident reconnaissance data exist, the intensity and radii estimative algorithms may be redeveloped so that they are based entirely on ground truth, making them completely independent of the Dvorak method.

Acknowledgments. The authors thank Dr. James Purdom for instigating this work and providing initial funding, Dr. Mitch Goldberg for creating the temperature retrieval, and Dr. Stan Kidder for useful discussions and assistance with data acquisition. This research was partially funded by an AMS Graduate Student Fellowship, sponsored by DynCorp, and also by the U.S. Weather Research Program, NOAA Grants NA67RJ0152 and NA17RJ1228.

APPENDIX

Development of CLW and Ice Corrections

To represent more accurately the retrieved tropical-cyclone temperature, pressure, and wind fields, a correction for hydrometeor effects in necessary. Modifications for absorption in areas of high CLW content and scattering by ice were developed, based upon the method described by Linstid (2000).

Both corrections are implemented at 12 pressure levels between 350 and 920 hPa (i.e., 350, 400, 430, 475, 500, 570, 620, 670, 700, 780, 850, and 920 hPa) at which AMSU temperatures are retrieved. As will be seen, the attenuation effects of CLW at the lower pressure levels are minimal, so that only a correspondingly slight adjustment is done. The data used in developing the correction come from 64 AMSU passes over Atlantic and east Pacific storms from the 1999 tropical season. Despite the 154 total passes over tropical disturbances that year, only those are used for which the analysis domain is completely over the ocean in order to provide homogeneity in the sample.

a. CLW correction

The basis of the CLW correction is to remove the artificial relationship between lower derived temperatures and large amounts of CLW by using the temperature and CLW data associated with each footprint. The temperature data utilized in the correction consist of all AMSU footprints within a 12° × 12° storm-centered grid.

At each pressure level, the mean temperature T_{mean} of all the swath points is calculated for each storm and is used to find the temperature deviation T_{dev} at each footprint i by subtracting the actual temperature T at that footprint:

$$T_{\text{dev}}(i) = T_{\text{mean}} - T(i). \qquad \text{(A1)}$$

A linear regression then is performed at each of the 12 pressure levels, using the data points from all 64 AMSU passes with the temperature deviations as the dependent variable and the associated CLW values as the independent variable. Next, the slopes of the 12 regression lines are plotted against their corresponding pressure level m_p, and a quadratic curve is fit to the data (Fig. A1). At 350 hPa, the slope is nearly zero, indicating that CLW does not affect temperature because there is less CLW at this level. In contrast, the magnitude of the slope is largest at 920 hPa, representing the decrease in temperature due to the abundance of CLW at this level.

Not all swath points are affected by CLW, and so only those with a corresponding CLW value greater than 0.3 mm are corrected for attenuation effects. The correction is given by

$$T_{\text{corrected}}(i) = T_{\text{original}}(i) + m_p\text{CLW}(i), \qquad \text{(A2)}$$

where $T_{\text{corrected}}$ is the corrected temperature at each footprint, T_{original} is the uncorrected temperature, and m_p is the slope for a given pressure level.

b. Ice correction

After the CLW correction, the temperature data are corrected further for scattering by ice crystals with the

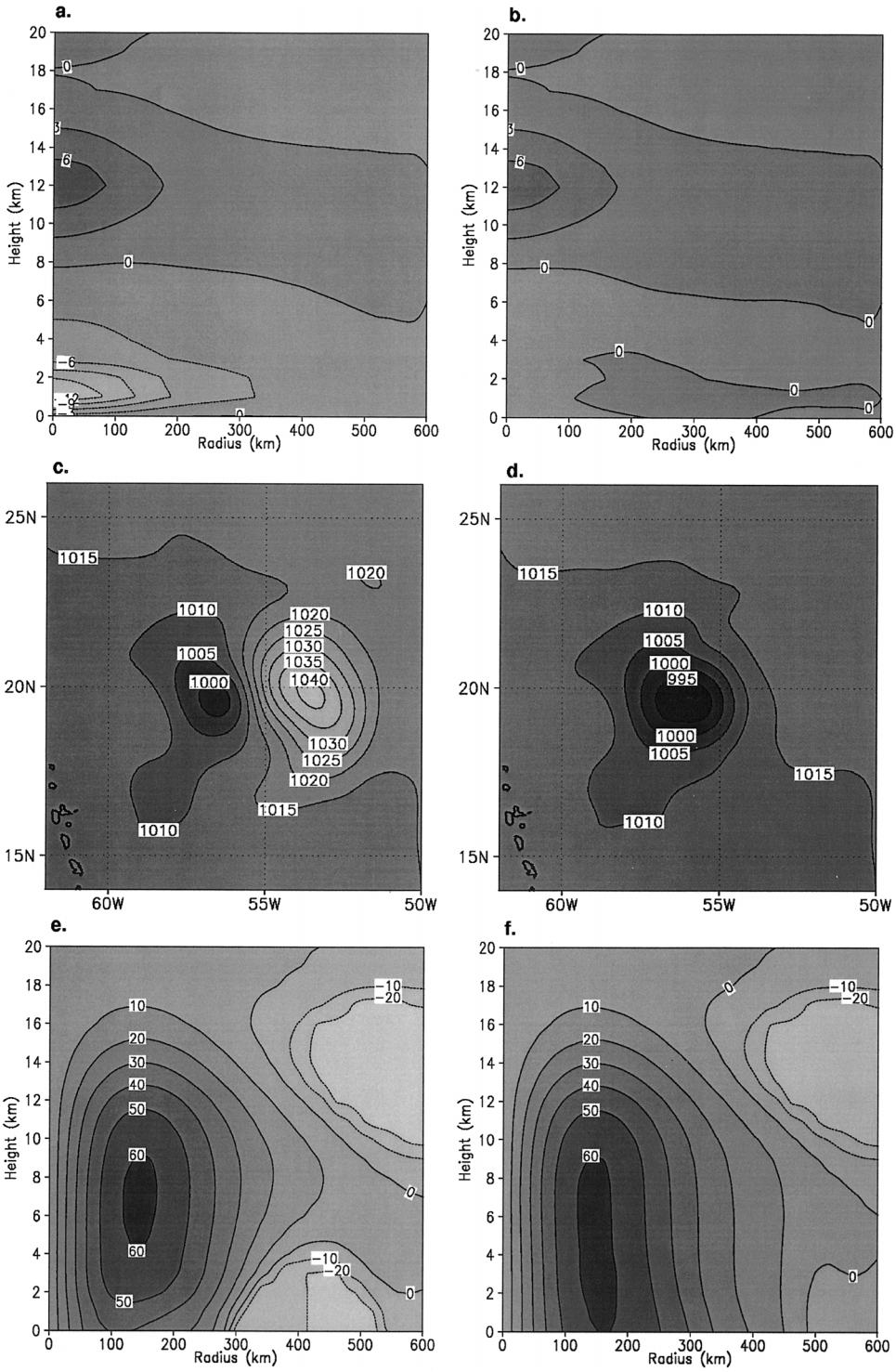

FIG. A2. (a), (c), (e) Non-hydrometeor-corrected and (b), (d), (f) hydrometeor-corrected plots for Hurricane Gert (115 kt) from 1148 UTC 17 Sep 1999, showing (a), (b) radial–height cross section of temperature anomalies (°C), (c), (d) lat × lon profile of surface pressure (hPa), and (e), (f) radial–height profile of azimuthally averaged gradient wind (kt).

method described by Linstid (2000) with minor modifications. Prior to the ice correction, a distance-weighted averaging method (Barnes 1964) is used to interpolate the unevenly spaced swath data to an evenly spaced 12° × 12° grid with 0.2° grid spacing. It would be preferable to perform the ice correction on the swath data, as with the CLW correction, because the Barnes analysis smoothes the data. However, the Laplacian method utilized by Linstid (2000), described as follows, requires that the data be evenly spaced.

At each of the 12 aforementioned pressure levels, the mean temperature, unaffected by ice, is calculated by only using points at which the associated CLW value is less than 0.2 mm. This constraint is based on the assumption that cloud ice does not occur where there is little or no CLW. If the temperature at a given grid point is less than the mean temperature minus 0.5°C, the data point is considered to be too cold because of ice attenuation, and it is flagged to be corrected.

Following Linstid (2000), once all of the points affected by ice are flagged at each pressure level, Laplace's equation [(A3)]—where T is the temperature—is used to fix the corrupted data, because it provides a smooth temperature field using uncorrupted data points:

$$\nabla^2 T = 0. \tag{A3}$$

Equation (A3) is solved by iteratively replacing each flagged data point with the average of its nearest neighbors, of which there are four if the point is in the center of the domain, three if it is on the side, and two if it is in the corner. This correction procedure is continued until the temperatures of all the flagged data points converge such that the differences in the temperatures between the previous and current iteration are less than 0.005°C.

In Fig. A2 are the uncorrected versus the hydrometeor-corrected plots of the radial–height cross sections of temperature anomaly (°C) and azimuthally averaged gradient wind (kt), as well as the horizontal distribution of surface pressure (hPa) of Hurricane Gert when it was a category-4 storm with an MSW of 115 kt. The corrections greatly reduced the large area of low-level cold temperatures and the large area of surface high pressure. The adjusted wind profile is much more realistic than the uncorrected version, with the low-level anticyclonic area at the storm's edge removed.

REFERENCES

Bankert, R. L., and P. M. Tag, 2002: An automated method to estimate tropical cyclone intensity using SSM/I imagery. *J. Appl. Meteor.*, **41,** 461–472.

Barnes, S., 1964: A technique for maximizing details in numerical weather map analysis. *J. Appl. Meteor.*, **3,** 396–409.

Brown, D. P., and J. L. Franklin, 2002: Accuracy of pressure–wind relationships and Dvorak satellite intensity estimates for tropical cyclones determined from recent reconnaissance-based ''best track'' data. Preprints, *25th Conf. on Hurricanes and Tropical Meteorology*, San Diego, CA, Amer. Meteor. Soc., 458–459.

Brueske, K. F., and C. S. Velden, 2003: Satellite-based tropical cyclone intensity estimation using the NOAA-KLM series Advanced Microwave Sounding Unit (AMSU). *Mon. Wea. Rev.*, **131,** 687–697.

Depperman, C. E., 1947: Notes on the origin and structure of Philippine typhoons. *Bull. Amer. Meteor. Soc.*, **28,** 399–404.

Dvorak, V. F., 1975: Tropical cyclone intensity analysis and forecasting from satellite imagery. *Mon. Wea. Rev.*, **103,** 420–430.

——, 1984: Tropical cyclone intensity analysis using satellite data. NOAA Tech. Rep. NESDIS 11, 47 pp. [Available from National Technical Information Service, U.S. Department of Commerce, Sills Bldg., 5285 Port Royal Rd., Springfield, VA 22161.]

Goldberg, M. D., D. S. Crosby, and L. Zhou, 2001: The limb adjustment of AMSU-A observations: Methodology and validation. *J. Appl. Meteor.*, **40,** 70–83.

Jones, W. L., V. J. Cardone, W. J. Pierson, J. Zec, L. P. Rice, A. Cox, and W. B. Sylvester, 1999: NSCAT high-resolution surface wind measurements in Typhoon Violet. *J. Geophys. Res.*, **104,** 11 247–11 259.

Kidder, S. Q., 1979: Determination of tropical cyclone surface pressure and winds from satellite microwave data. Ph.D. dissertation, Colorado State University, 87 pp.

——, and T. H. Vonder Haar, 1995: *Satellite Meteorology: An Introduction.* Academic Press, 466 pp.

——, W. M. Gray, and T. H. Vonder Haar, 1978: Estimating tropical cyclone central pressure and outer winds from satellite microwave data. *Mon. Wea. Rev.*, **106,** 1458–1464.

——, ——, and ——, 1980: Tropical cyclone outer surface winds derived from satellite microwave sounder data. *Mon. Wea. Rev.*, **108,** 144–152.

——, M. D. Goldberg, R. M. Zehr, M. DeMaria, J. F. W. Purdom, C. S. Velden, N. C. Grody, and S. J. Kusselson, 2000: Satellite analysis of tropical cyclones using the Advanced Microwave Sounding Unit (AMSU). *Bull. Amer. Meteor. Soc.*, **81,** 1241–1259.

Knaff, J. A., R. M. Zehr, M. D. Goldberg, and S. Q. Kidder, 2000: An example of temperature structure differences in two cyclone systems from the Advanced Microwave Sounding Unit. *Wea. Forecasting*, **15,** 476–483.

Linstid, B., 2000: An algorithm for the correction of corrupted AMSU temperature data in tropical cyclones. M.S. thesis, Dept. of Mathematics, Colorado State University, 24 pp.

Merrill, R. T., 1995: Simulations of physical retrieval of tropical cyclone thermal structure using 55-GHz band passive microwave observations from polar-orbiting satellites. *J. Appl. Meteor.*, **34,** 773–787.

Schwerdt, R. W., F. P. Ho, and R. R. Watkins, 1979: Meteorological criteria for standard project hurricane and probable maximum hurricane wind fields, Gulf and East Coasts of the United States. NOAA Tech. Rep. NWS 23, 317 pp.

Spencer, R. W., and W. D. Braswell, 2001: Atlantic tropical cyclone monitoring with AMSU-A: Estimation of maximum sustained wind speeds. *Mon. Wea. Rev.*, **129,** 1518–1532.

Velden, C. S., T. L. Olander, and R. M. Zehr, 1998: Development of an objective scheme to estimate tropical cyclone intensity from digital geostationary satellite infrared imagery. *Wea. Forecasting*, **13,** 172–186.

Weatherford, C., and W. M. Gray, 1988: Typhoon structure as revealed by aircraft reconnaissance. Part II: Structural variability. *Mon. Wea. Rev.*, **116,** 1044–1056.